Estimating the dopant distribution in Ca-doped α-SiAlON: statistical HAADF-STEM analysis and large-scale atomic modeling

Norihito Sakaguchi*, Fuuta Yamaki, Genki Saito, Yuji Kunisada

Laboratory of Integrated Function Materials, Center for Advanced Research of Energy and Materials, Faculty of Engineering, Hokkaido University

Kita-13, Nishi-8, Kita-ku, Sapporo, Hokkaido 060-8628, Japan

Running title: HAADF-STEM of Ca-doped α-SiAlON

***Corresponding author**

Norihito Sakaguchi

Tel & Fax: +81-11-706-6768

E-mail: sakaguchi@eng.hokudai.ac.jp

Kita-13, Nishi-8, Kita-ku, Sapporo, Hokkaido 060-8628, Japan

Total page: 15

# of Figures: 8

# of Tables: 1

Keywords: α-SiAlON, HAADF-STEM, multi-slice simulation, electron channeling, Monte Carlo simulation, dopant distribution

Abstract

We investigated the dopant distribution in Ca-doped α-SiAlON by using high-angle annular dark-field scanning transmission electron microscopy and a multi-slice image simulation. Our results showed that the electron wave propagated by hopping to adjacent Si(Al) and N(O) columns. The image intensities of the Ca columns had wider dispersions than other columns. To estimate the Ca distribution in the bulk material, we performed a Monte Carlo atomic simulation of the α-SiAlON with Ca dopants. A model including a short-range Coulomb-like repulsive force between adjacent Ca atoms reproduced the dispersion of the intensity distribution of the Ca column in the experimental image.

Introduction

α-SiAlON is a ceramic compound with the composition $M_xSi_{12-(m-n)}Al_{m-n}O_nN_{16-n}$ whose atomic structure is equivalent to α-Si_3N_4, replacing the Si–N bonds with Al–N and Al–O bonds. The notation M corresponds to cations such as Ca and Y, which dissolve into the interstitial (closed channel) sites in the unit cell to compensate for the crystal's charge imbalance. Figure 1 shows the unit cell of the a-SiAlON crystal. Each unit cell has two interstitial sites, indicated in the figure by arrows.

Ca-doped α-SiAlON is widely used as a structural ceramic because of its high mechanical strength, wear resistance, corrosion resistance, and oxidation resistance [1–6]. Recently, α-SiAlON has been predicted to exhibit highly efficient fluorescence when it is co-doped with a small amount of lanthanoid elements such as Eu and Ce [7–9]. To control the light emission of fluorescent α-SiAlON, it is necessary to assess the spatial distribution and cross-correlation of the dopants in the Si(Al)–N(O) network.

High-resolution transmission electron microscopy (HRTEM) is very useful for quantitatively analyzing the local atomic structure and composition of multicomponent compounds. HRTEM can obtain precise information on the atomic positions in a material, but it is difficult to use to identify the atomic species in specific sites.

Nevertheless, recent advances in high-angle annular dark-field scanning transmission electron microscopy (HAADF-STEM) enable us to investigate the local atomic structure using TEM, and many such highly

precise studies have been conducted for semiconductors, oxides, metallic compounds, and quasi-crystals [10–15].

In HAADF-STEM, image contrast is proportional to $Z^{1.6–2.0}$ (Z: atomic number) because thermal diffuse scattering (TDS) becomes the dominant scattering mechanism in electrons scattered at relatively high angles. This feature has been used to directly image dopants in host materials [16–18]. Studies of the precise interstitial site of dopants in α-SiAlON have revealed that their atomic positions vary slightly depending on the type of dopant [19–20]. However, these observations are effective only at very small dopant concentrations. The occupancy of Ca and Y needed to stabilize the α-SiAlON crystal is usually a few percent, making it difficult to directly observe the distribution of individual dopant atoms.

In the present study, we investigated the distribution of Ca dopants in α-SiAlON by using HAADF-STEM and an image simulation. Assessing the contrast change of the Ca atomic column among various arrays of Ca atoms, we attempted to find a plausible distribution of Ca.

Methods

First, Ca-doped α-SiAlON powders (Combustion Synthesis Co., Ltd., Japan) were sintered at 2073 K for 2 h by spark plasma sintering. Using energy-dispersive X-ray spectroscopy, the Ca concentration was estimated to be 1.3 at.%, which corresponds to an occupancy of 0.2 among all interstitial

sites shown in Figure 1. The sintered α-SiAlON block was sliced, mechanically polished down to a thickness of 20 μm, and ion milled with 3-kV Ar ions (PIPS model 691; Gatan Inc., USA). HAADF-STEM (Titan^3 G2 60-300; FEI Company) was then performed at 300 kV.

The inner correction semi-angle of the HAADF detector and the convergence semi-angle of the electron probe were 64 mrad and 22 mrad, respectively. The HAADF-STEM images and electron beam propagation behaviors were simulated with the Dr. Probe multi-slice (MS) image simulator [21], which incorporates the influence of TDS by using the frozen phonon approximation. In these image simulations, for the effective source distribution we used a Lorentzian function with a full width at half maximum of 0.06 nm. The defocus spread was set to 3 nm, and the C_S and other high-order aberrations were set to zero. For the MS simulation, 9600 Ca atoms were randomly dispersed among 480 000 interstitial sites in a supercell with dimensions of 12×14×46 nm. Two relaxed structures were calculated based on the Metropolis–Monte Carlo (MC) algorithm. In the MC simulation, the interactions between neighboring Ca atoms were modeled with screened Coulomb potentials.

Result and discussion

Figure 2 shows a typical HAADF-STEM image and an atomic model of Ca-doped α-SiAlON viewed from the [0001] direction. The brighter spots directly reflect the positions of each atomic column of Si(Al), N(O), and

Ca-N(O). There are two notable results in this HAADF image:

1) The intensity ratio of the adjacent Si1 and N1 columns was ~1.1, a value far from the ratio of the atomic numbers of each column.

2) The intensities of individual Ca columns varied considerably among measurement points.

Here, we introduce the relative intensity between each atomic columns and the N1 column: First, the background intensity was evaluated by averaging the intensities of five different darkest pixels in the image. After subtracting the background intensity from the original image, the peak intensity of every atomic column was measured. Finally, the measured intensities of all atomic columns were divided by the averaged intensity of the N1 column. Table 1 summarizes the relative intensity and standard deviation of each column. The standard deviation of the Ca column was twice that of the other columns. This result implies that the occupancy of Ca atoms was different in each column. These points are discussed further in the next section.

First, let us discuss the intensity ratio of the Si1 and N1 columns. Figure 3(a) shows a [0001]-projection atomic structure of Ca-doped α-SiAlON, and Fig. 3(b) and (c) show the corresponding simulated and experimental HAADF-STEM images, respectively. The intensity ratio of the Si1 and N1 columns was ~1.1 in both images. Although there were twice as many N(O) atoms in the N1 column as there were Si(Al) atoms in the Si1 column, a difference in atomic numbers for Si1 and N1 presumes that the Si1/N1

intensity ratio should be 1.5–2 according to the simplified z-dependence ($\propto Z^{1.6–2.0}$).

The intensity ratios of the experimental and simulated images are clearly smaller than the estimate, so we solve this discrepancy by assessing the channeling behavior of the electron beam propagation for each column. Figure 3(d) shows the behavior of the electron wave propagation when the convergent electron beam illuminates the N1 or Si1 column. The electron beam enters the upper surface of the sample (0 nm) and exits the lower surface (46 nm). The electron beam incident on the N1 column is immediately localized on the N1 column and then propagates along the N1 column; however, after propagating about 20 nm into the N1 column, the electron beam jumps to the adjacent Si1 column and propagates through it. Near the emission surface, the electron beam returns to the original N1 column.

The electron wave exhibits a similar dechanneling behavior when it is incident on the Si1 column. This behavior is similar to electron wave propagation into ß–Si_3N_4 [16] because α-SiAlON and ß–Si_3N_4 have similar crystal structures. Thus, the image intensities in the Si1 and the N1 columns appeared to grow closer to these average values. In addition, the MS calculation indicated that the intensity ratios of the Si1/N1 column and other columns strongly depended on the sample thickness. By comparing these intensity ratios to the experimental values, we estimated the sample thickness to be 46 nm.

Now, we shall consider the causes of dispersion in the Ca column intensity. In simple terms, this dispersion is influenced by the differences in the numbers of Ca atoms among the columns. The occupancy of Ca atoms is 0.2, but individual columns should have different numbers of Ca atoms, so the intensities of the Ca column were dispersed. However, it was difficult to directly determine the numbers of Ca atoms in individual columns from the image.

Now, let us explain this difficulty using Fig. 4, which shows simulated HAADF images with 15 Ca atoms in the Ca column in various Ca distributions (periodic array and random distribution). The corresponding propagation behaviors of the electron wave are shown in the lower part of the figure, revealing that the intensities of the Ca columns were not the same. When there is much Ca near the top surface, the intensity of the Ca column strengthens, but the intensity weakens when Ca atoms are present near the bottom surface. The change in this intensity ratio corresponds to a difference of 1–2 Ca atoms. In other words, this result means that an error of ~10% exists when the number of Ca atoms is directly determined from the image intensity at the present sample thickness.

As mentioned before, we could not directly determine the number of Ca atoms in the Ca column from the image intensity, so we estimated a plausible spatial distribution of Ca atoms as follows: 9600 Ca atoms were randomly placed in a supercell of 24000 SiAlON unit cells (48000 Ca interstitial sites), as shown in Fig. 5(a). Then, the equilibrium Ca

distribution at the sintering temperature of 2073 K was calculated by the MC method using the screened Ca–Ca Coulomb potentials (E_{pair}):

$$E_{pair} = \frac{n^2}{4\pi\varepsilon_0}\frac{e^2}{r} \times \exp\left(-\frac{r}{r_s}\right),$$

where n is the valence number of Ca, e is the elementary charge, ε_0 is the permittivity of vacuum, r is the distance between two Ca atoms, and r_s is the screening distance for the screening effect of the surrounding Si(Al)–N(O) network. Figure 5(b) shows the shape of the potential curve. In each MC step, we randomly chose a Ca atom and moved it to other interstitial sites, then calculated the total energy of the cell. Here, we ignored the influence of lattice vibrations and only considered the screening effect in the interaction between Ca atoms and other elements. The screening distance of the Coulomb potential was set to be 3 nm or infinity (no screening).

Figure 6(a) shows the radial distribution function (RDF) for the Ca atoms before and after structural relaxation. The shape of the RDF for the random Ca distribution corresponds to the RDF of the Ca interstitial site itself, which indicates that the fraction of the first nearest neighbor Ca atoms is higher than that of all further neighbors. In contrast, after relaxation, the proportions of the first and second nearest neighbor Ca atoms decrease, and the proportions of the third and fourth nearest neighbor atoms tend to increase. Particularly, this shows that the few first and second nearest neighbor Ca atoms existed after structural relaxation, using the pair potential with a screening distance of 3 nm.

Figure 6(b) shows the appearance frequency of the Ca atoms in each column. The dispersion in the number of Ca atoms in individual columns tended to narrow after structural relaxation with a screening distance of 3 nm. The HAADF-STEM images were then calculated over a 4.7×5.4×46 nm region of the initial and relaxed supercells, as shown in Fig. 5(a). Figure 7 shows these results with the experiment image. In all images, the changes in the Ca column intensity well reproduced those in the experimental image.

Figure 8 shows the intensity distributions of each column (Si1, N1, N2, and Ca) measured from the HAADF images. In the experimental image, the intensity distributions of the Si1, N1, and N2 columns also show slight spreading as a result of quantum noise and equipment instability. Thus, we convoluted a Gaussian function with a standard deviation of 0.03 for the calculated intensity distribution profiles. The deviation value was optimized by fitting the Si, N1, and N2 distributions in the experimental results. The experimental image in Fig. 8(a) reveals that the Ca column had a much wider intensity distribution than the other columns. This tendency also appears in the calculated intensity distributions in Fig. 8(b)–(d), and the dispersions of the distribution for the random distribution and the relaxed structure without screening become larger than that in the experimental image. However, the dispersion of the intensity distribution of the Ca column using the screened pair potential almost agrees with that of the experimental image, suggesting that it reproduced the atomic model corresponding to the plausible Ca distribution.

These results indicate that the Ca atoms dissolve in the interstitial sites of α-SiAlON as divalent cations, and that a Coulomb-like repulsive force exists between adjacent Ca atoms. They also suggest that the Coulomb repulsion is limited to a short range by screening from the surrounding Si(Al)–N(O) networks. The RDF indicates that there is no Ca atom within 0.8 nm of another Ca atom. This knowledge is important in interpreting the atomic interactions in co-doped (e.g., Ca, Y, and Eu) fluorescent α-SiAlON, and in future work we will investigate the dopant distribution in fluorescent α-SiAlON by using this technique.

Concluding remarks

Using HAADF-STEM, we investigated the dopant distribution in Ca-doped α-SiAlON. The intensity ratio of adjacent Si1 and N1 columns was far from the ratio of the atomic numbers of each column because there was dechanneling of the electron wave between these columns. The individual Ca–N(O) columns showed wider intensity dispersion than other columns. Using a MC simulation, we estimated a plausible spatial distribution of Ca atoms in the α-SiAlON. Found from a MC simulation using the screened Coulomb potential, the calculated dispersion of the intensity distribution of the Ca column nearly agreed with the experimental image. This result indicates that a short-range Coulomb-like repulsive force exists between adjacent Ca atoms in the α-SiAlON network.

Acknowledgments

We thank Mr. Harada for providing the α-SiAlON powders. We also gratefully acknowledge Mr. K. Ohkubo, Mr. R. Oota, Mr. T. Tanioka, and Ms. Yamanouchi for their technical support in TEM operations. A part of this work was conducted at Hokkaido University, supported by the "Nanotechnology Platform" Program of the Ministry of Education, Culture, Sports, Science and Technology (MEXT), Japan. This work was also supported by JSPS KAKENHI (Grant Number 26249098).

References

1. Wang P L, Zhang C, Sun W Y, Yan D S (1999) Characteristics of Ca-α-sialon—Phase formation, microstructure and mechanical properties. *J. European Ceramic Society* 19: 553–560.

2. Kurama S, Herrmann M, Mandal H (2002) The effect of processing conditions, amount of additives and composition on the microstructures and mechanical properties of α-SiAlON ceramics. *J. European Ceramic Society* 22: 109–119.

3. Ye F, Hoffmann M J, Holzer S, Zhou Y, Iwasa M (2003) Effect of the amount of additives and post-heat treatment on the microstructure and mechanical properties of yttrium–α-sialon ceramics. *J. American Ceramic Society* 86: 2136–2142.

4. Jonesa M I, Hirao K, Hyuga H, Yamauchi Y, Shen Z, Nygren M (2004) Wear properties of self-reinforced α-SiAlON ceramics produced by spark

plasma sintering. *Wear* 257: 292–296.

5. Nagae M, Koyama Y, Yasutake S, Yoshio T, Oda K (2006) Corrosion behavior of sialon ceramics in supercritical water. *J. American Ceramic Society* 89: 3550–3553.

6. Yu J, Du H, Shuba R, Chen I-W (2004) Dopant-dependent oxidation behavior of α-SiAlON ceramics. *J. Mater. Sci.* 39: 4855–4860.

7. Krevel J W H, Rutten J W T, Mandal H, Hintzen H T, Metselaar R (2002) Luminescence properties of terbium-, cerium-, or europium-doped α-sialon materials. *J. Solid State Chem.* 165: 19–24.

8. Xie R J, Hirosaki N, Mitomo M, Yamamoto Y, Suehiro T, Sakuma K (2004) Optical properties of Eu^{2+} in α-SiAlON. *J. Phys. Chem. B* 108: 12027-12031.

9. Xu X, Tang J Y, Nishimura T, Hao L Y (2011) Synthesis of Ca-α-SiAlON phosphors by a mechanochemical activation route. *Acta Materialia* 59: 1570–1576.

10. Klenov D O, Zide J M, Zimmerman J D, Gossard A C, Stemmer S (2005) Interface atomic structure of epitaxial ErAs layers on „001… $In_{0.53}Ga_{0.47}As$ and GaAs. *Appl. Phys. Lett.* 86: 241901.

11. Huang C, Wu S, Sanchez A M, Peters J J P, Beanland R, Ross J S, Rivera P, Yao W, Cobden D H, Xu X1 (2014) Lateral heterojunctions within monolayer $MoSe_2$–WSe_2 semiconductors. *Nature Materials* 13: 1096–1101.

12. Saito M, Kimoto K, Nagai T, Fukushima S, Akahoshi D, Kuwahara H, Matsui Y, Ishizuka K (2009) Local crystal structure analysis with 10-pm accuracy using scanning transmission electron microscopy. *J. Electron*

Microsc. 58. 131–136.

13. Kishida K, Yokobayashi H, Inui H, Yamasaki M, Kawamura Y (2012) The crystal structure of the LPSO phase of the 14*H*-type in the Mg–Al–Gd alloy system. *Intermetallic*s 31: 55–64.

14. Ishimasa T, Iwami S, Sakaguchi N, Oota R, Mihalkovič M (2015) Phason space analysis and structure modelling of 100 Å-scale dodecagonal quasicrystal in Mn-based alloy. *Phil. Mag.* 95: 3745–3767.

15. Seki T, Abe E (2015) Local cluster symmetry of a highly ordered quasicrystalline $Al_{58}Cu_{26}Ir_{16}$ extracted through multivariate analysis of STEM images. *Microscopy* 64: 341–349.

16. Kimoto K, Xie R-J, Matsui Y, Ishizuka K, Hirosaki N (2009) Direct observation of single dopant atom in light-emitting phosphor of β-SiAlON:Eu^{2+}. *Appl. Phys. Lett.* 94: 041908.

17. Ishikawa R, Shibata N, Oba F, Taniguchi T, Findlay S D, Tanaka I, Ikuhara Y (2013) Functional complex point-defect structure in a huge-size-mismatch system. *Phys. Rev. Lett.* 110: 065504.

18. Ishikawa R, Lupini A R, Oba F, Findlay S D, Shibata N, Taniguchi T, Watanabe K, Hayashi H, Sakai T, Tanaka I, Ikuhara Y, Pennycook S J (2014) Atomic structure of luminescent centers in high-efficiency Ce-doped w-AlN single crystal. *Scientific Reports* 4: 3778.

19. Xu F, Sourty E, Shi W, Mou X, Zhang L (2011) Direct observation of rare-earth ions in α-sialon:Ce phosphors. *Inorg. Chem.* 50: 2905–2910.

20. Yurdakul H, Idrobo J C, Pennycook S J, Turan S (2011) Towards atomic

scale engineering of rare-earth-doped SiAlON ceramics through aberration-corrected scanning transmission electron microscopy. *Scripta Mater.* 65: 656–659.

21. Barthel J, Dr Probe – STEM multi-slice image calculation program, (http://www.er-c.org/barthel/drprobe).

Figure and Table captions:

Table 1 Relative intensity and standard deviation in each column.

Fig. 1 Crystal structure of α-SiAlON.

Fig. 2 HAADF-STEM image and atomic model of [0001] Ca-doped α-SiAlON.

Fig. 3 (a) Atomic model, (b) MS simulated image, and (c) experimental HAADF image of Ca-doped α-SiAlON. The channeling behaviors along the N1 and Si1 columns are shown in (d).

Fig. 4 (a) MS images of Ca-doped α-SiAlON with various Ca distributions. The channeling behaviors along the Ca column are shown in (b).

Fig. 5 Determination of the (a) super cell and (b) atomic potential used in the MC simulation.

Fig. 6 (a) Radial distribution function and (b) distribution of Ca number along the z-axis before and after the MC calculation.

Fig. 7 (a) Experimental and (b, c, d) calculated HAADF images of Ca-doped α-SiAlON with various Ca distributions.

Fig. 8 Intensity distribution of each column (Si1, N1, N2, and Ca) measured from the HAADF images in Fig. 6. Also shown are the dispersions of the Ca column intensity.

Table 1

Column	relative intensity	standard deviation
Si1	1.14	0.09
N1	1.00	0.11
N2	0.73	0.07
Ca	0.64	0.19

Fig.1

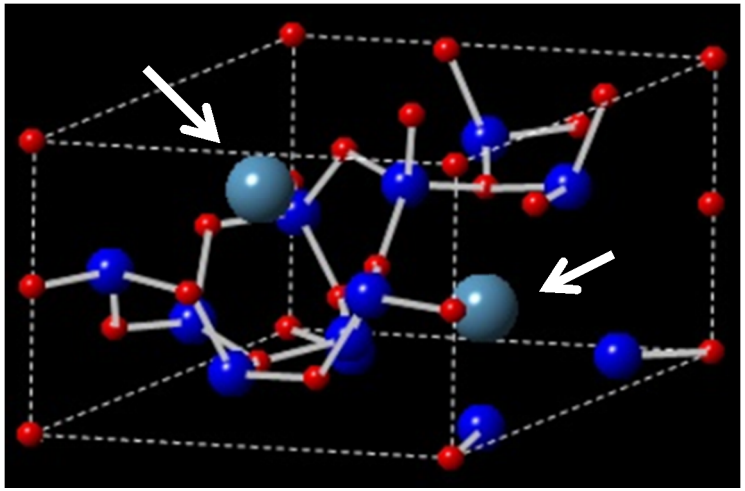

Interstitial site (Ca, Y)

Si, Al

O, N

Fig.2

*Ca occupancy : 0.2

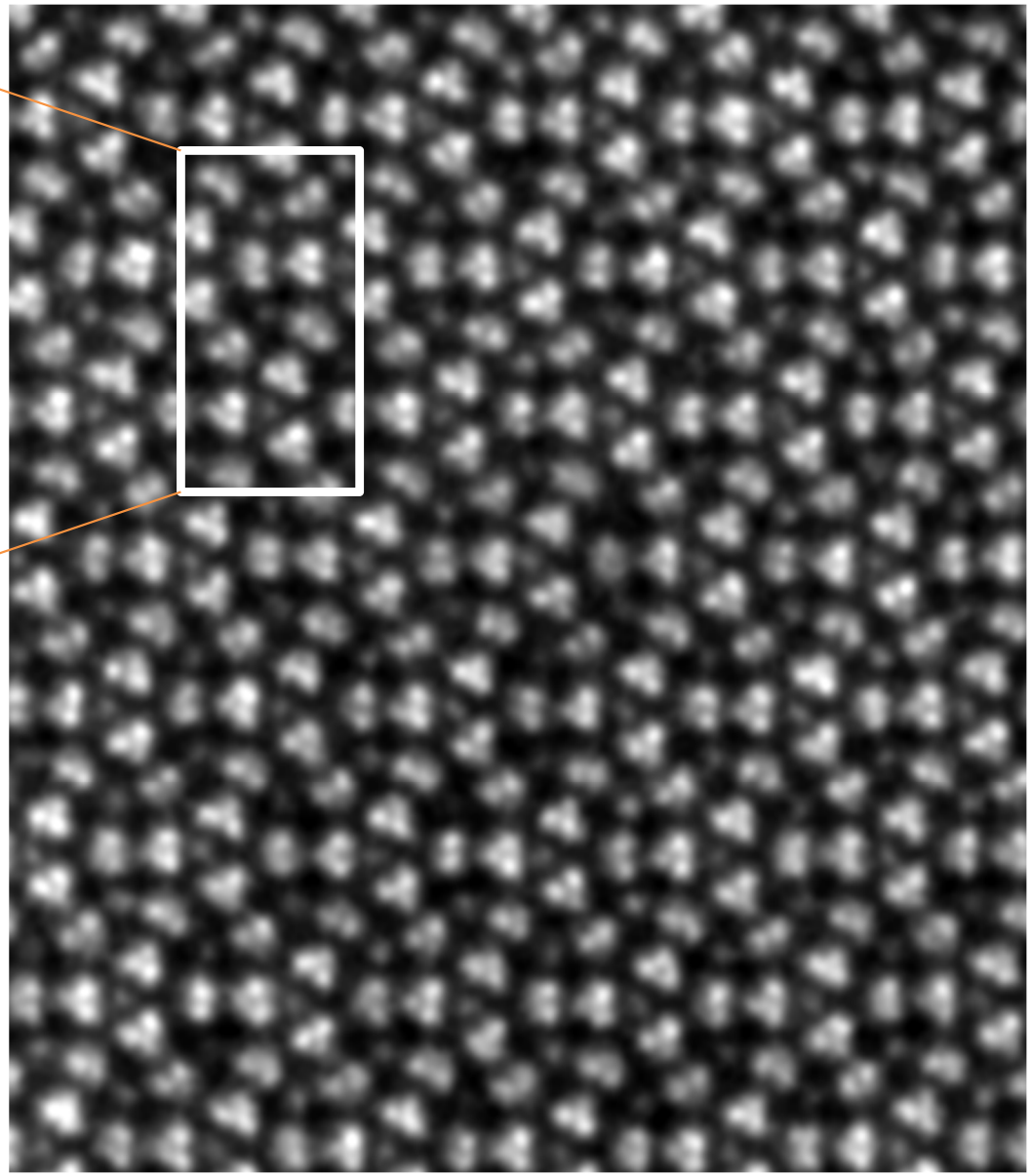

Fig.3

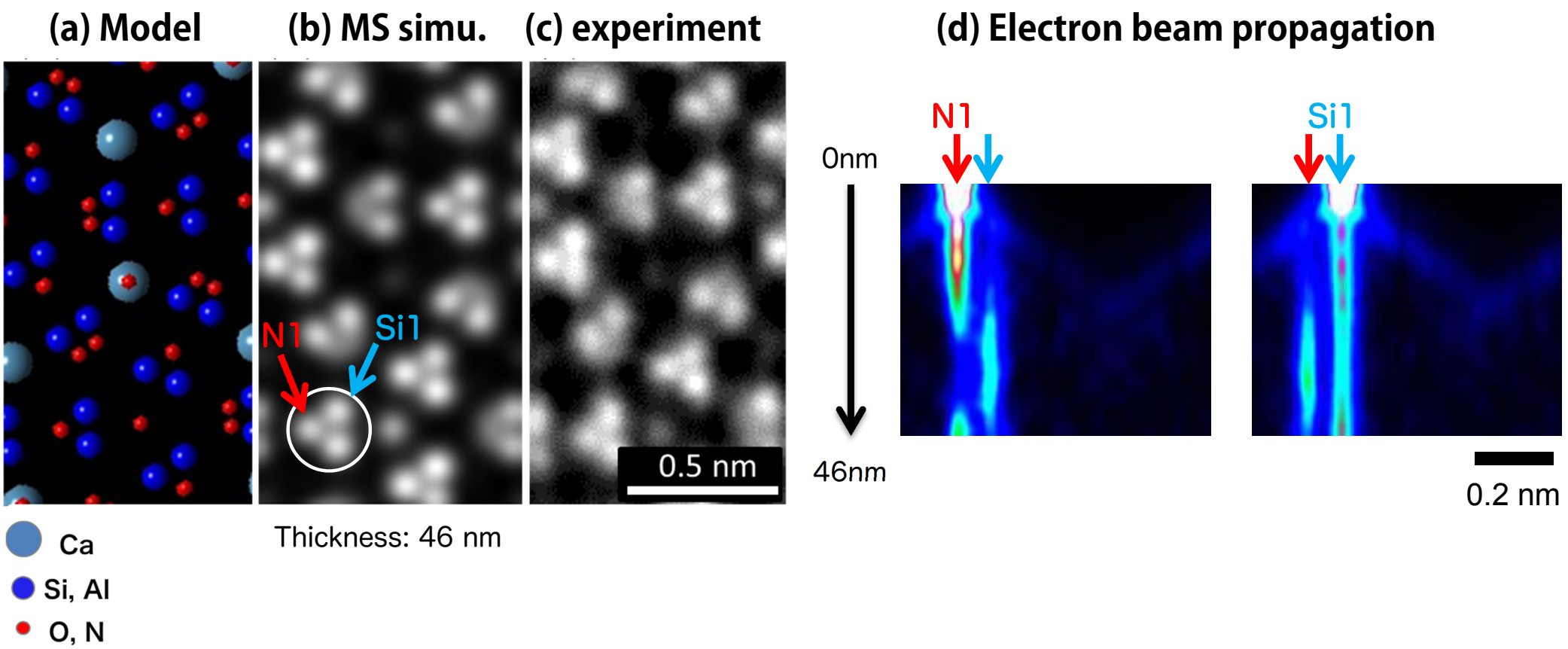
(a) Model
(b) MS simu.
(c) experiment
(d) Electron beam propagation
N1
Si1
0.5 nm
Thickness: 46 nm
Ca
Si, Al
O, N
0nm
46nm
N1
Si1
0.2 nm

Fig.4

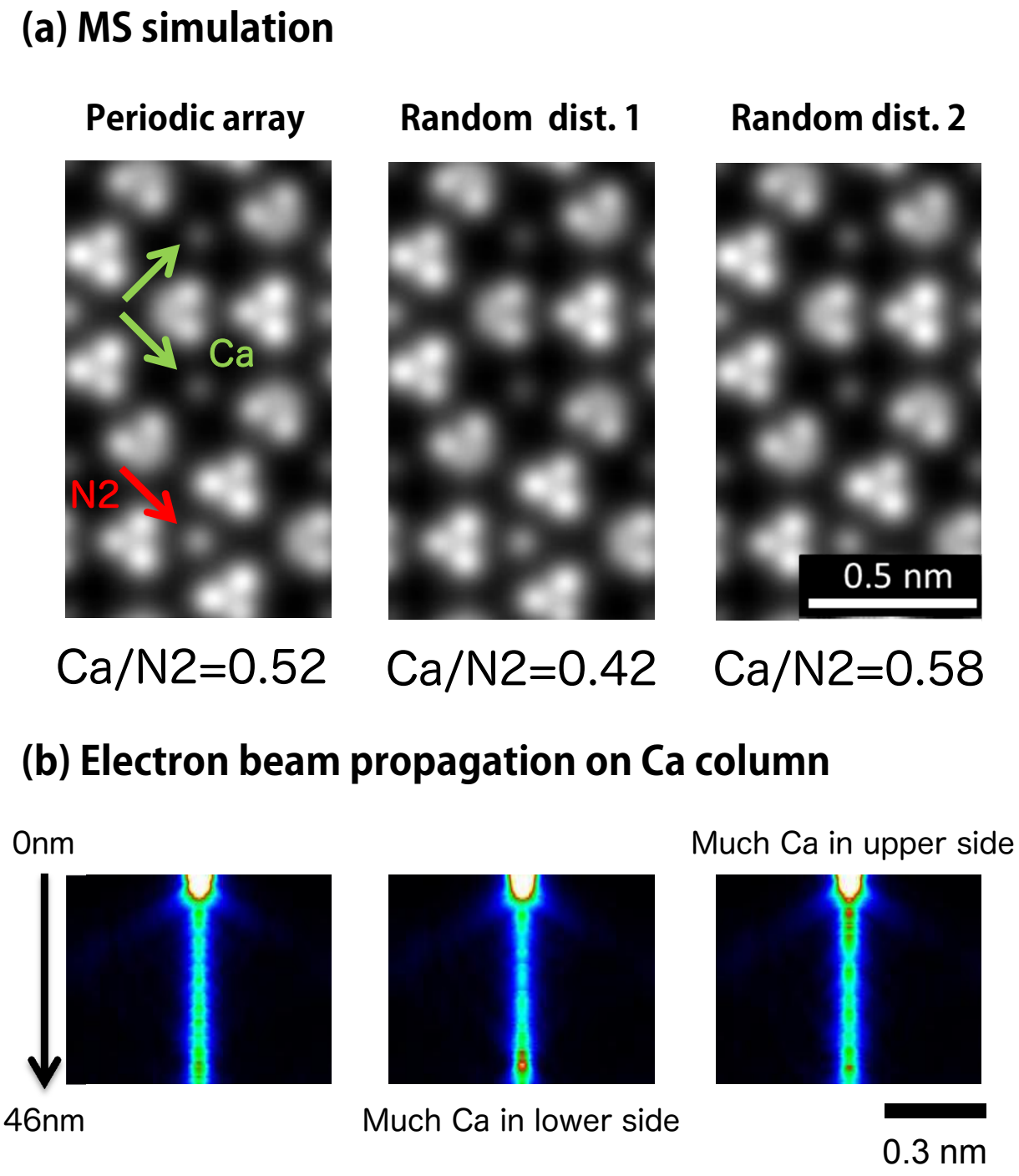
(a) MS simulation
Periodic array
Random dist. 1
Random dist. 2
Ca
N2
0.5 nm
Ca/N2=0.52
Ca/N2=0.42
Ca/N2=0.58
(b) Electron beam propagation on Ca column
0nm
46nm
Much Ca in lower side
Much Ca in upper side
0.3 nm

Fig.5

(a) Super cell

12nm×14nm×46nm
(24000 unit cells)

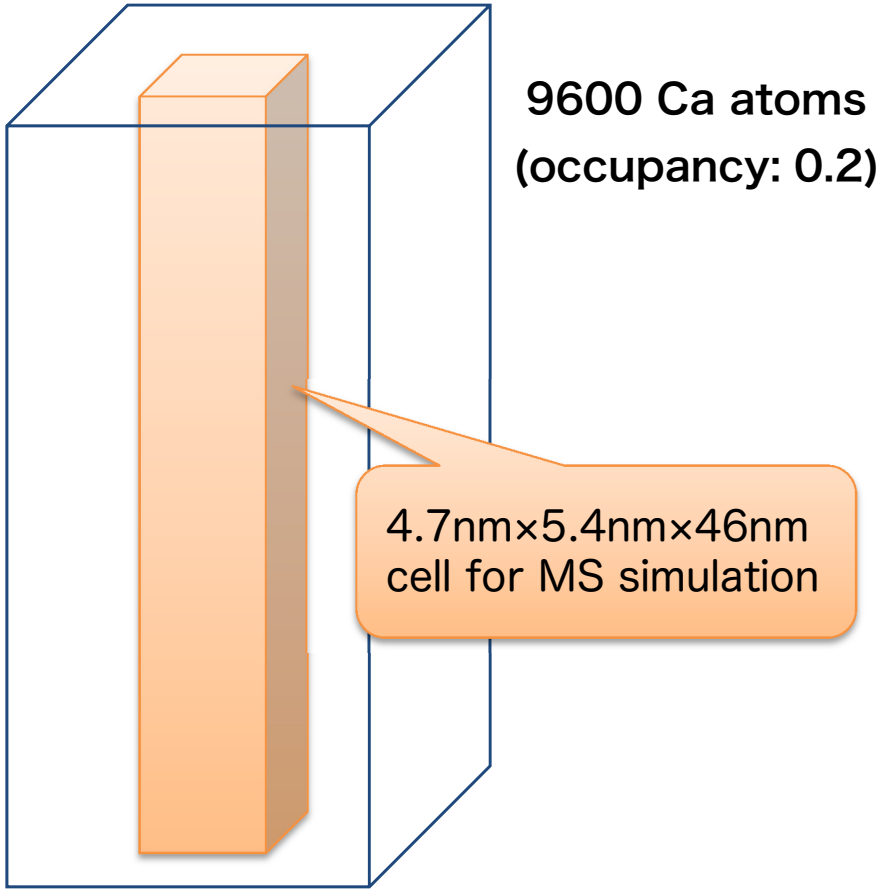

(b) Atomic potential

$$E_{pair} = \frac{n^2}{4\pi\varepsilon_0}\frac{e^2}{r} \times \exp\left(-\frac{r}{r_s}\right)$$

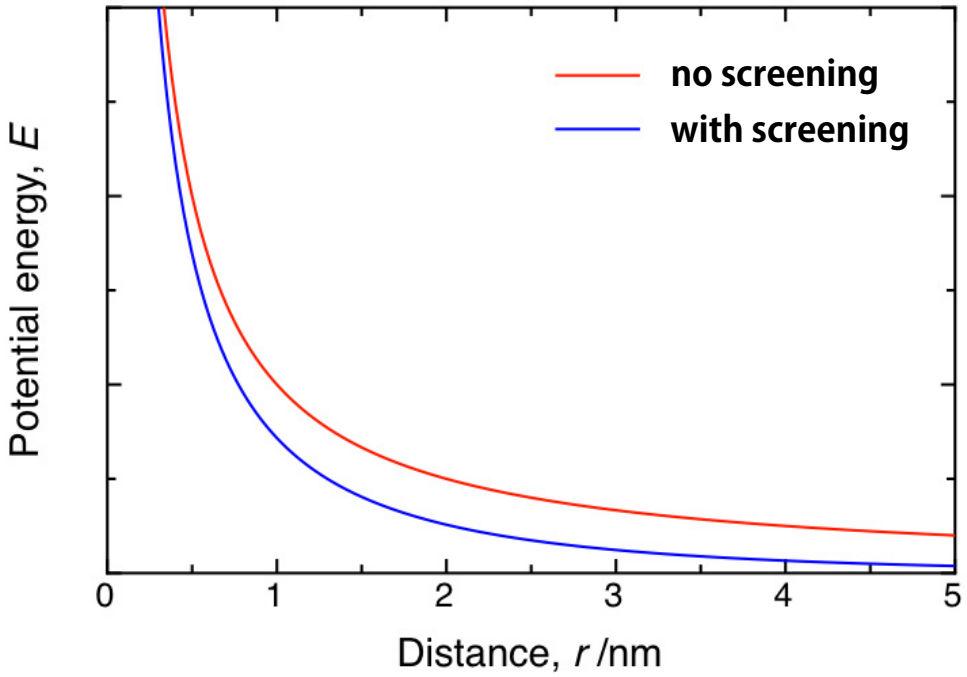

Fig.6

(a) Radial distribution function

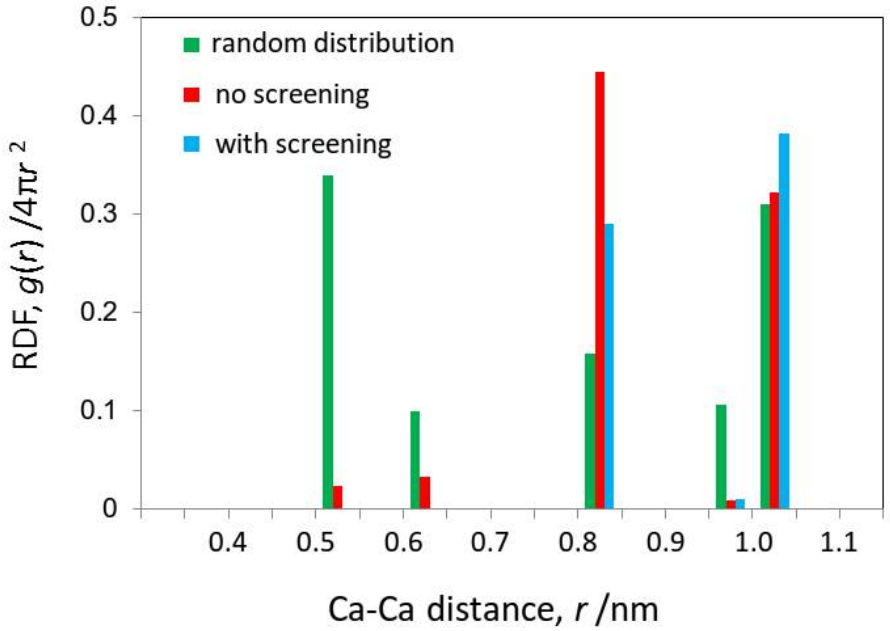

(b) Fraction of Ca numbers along z-axis

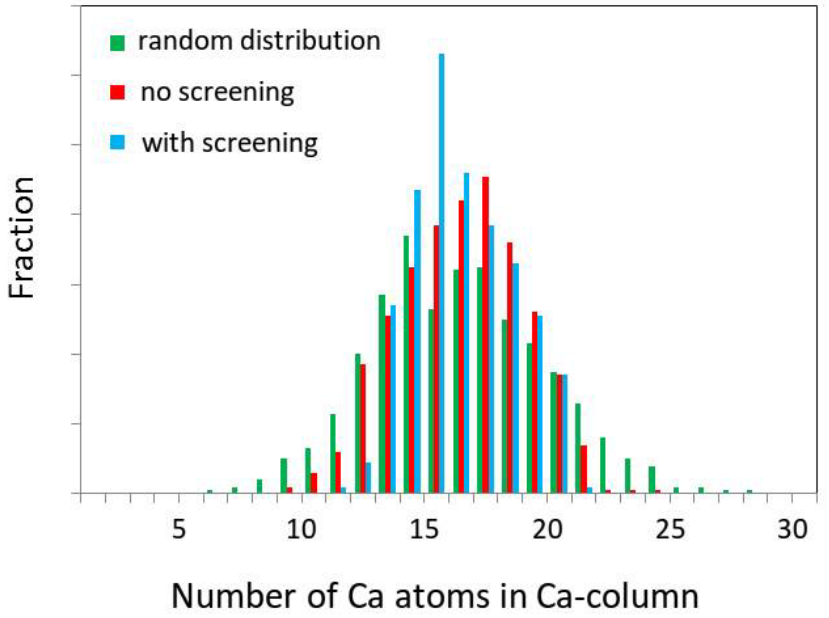

Fig.7

(a) experiment

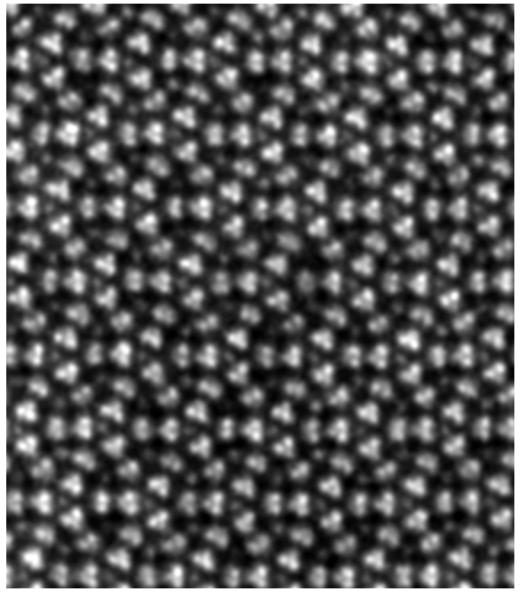

1 nm

(b) random dist.

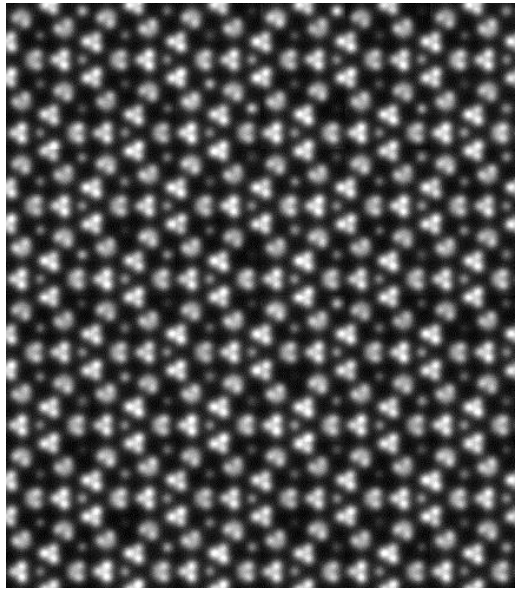

(c) relaxed structure 1
(no screening)

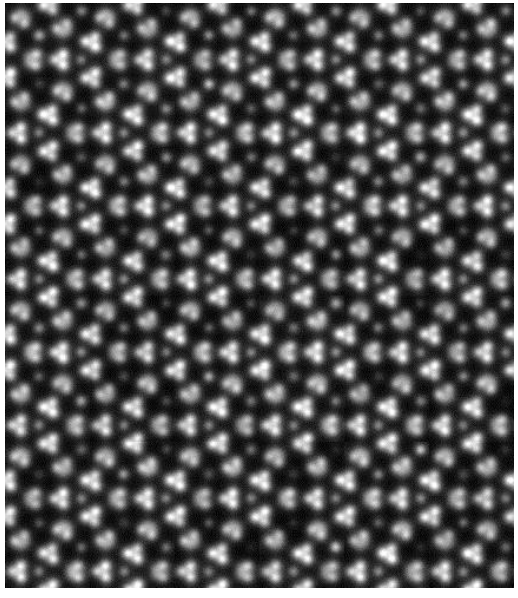

(d) relaxed structure 2
(with screening)

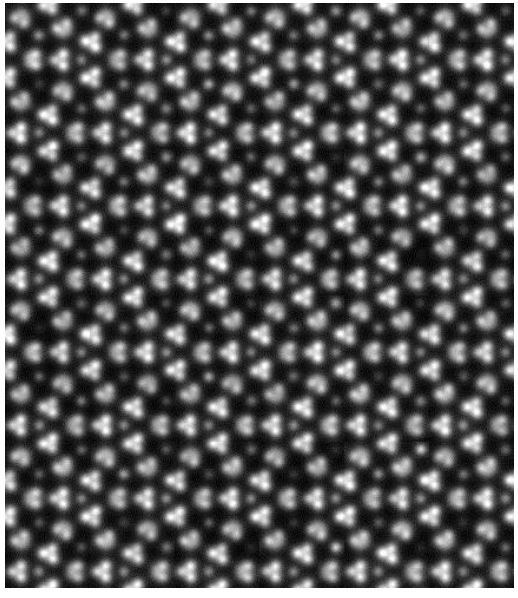

Fig.8

(a) experiment

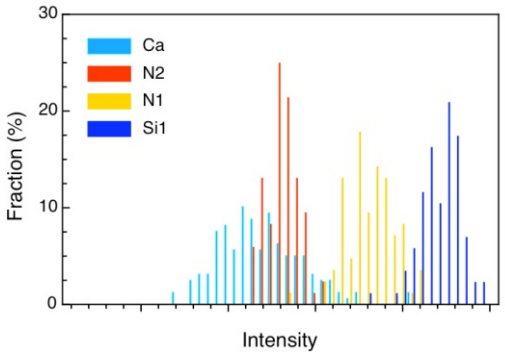

σ_{Ca}=0.19

(b) random dist.

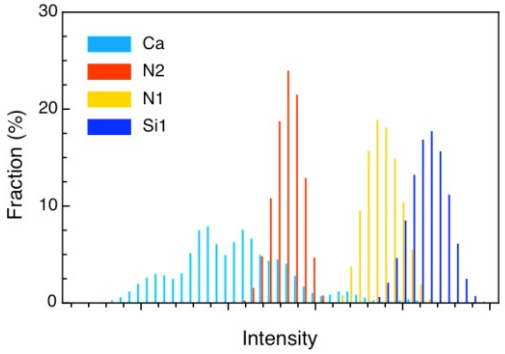

σ_{Ca}=0.23

(c) relaxed structure 1 (no screening)

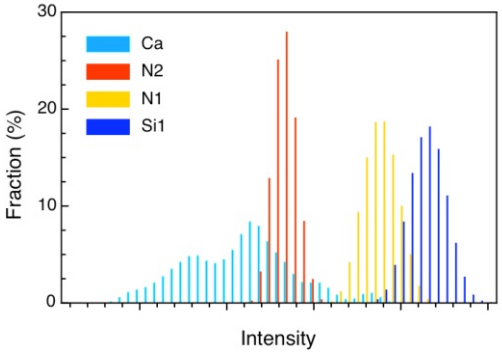

σ_{Ca}=0.24

(d) relaxed structure 2 (with screening)

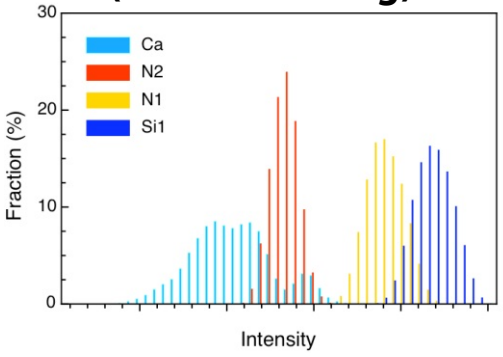

σ_{Ca}=0.18